MODELING AUTONOMOUS ENERGY SYSTEMS CONSISTING OF BIO-INSPRIED FUEL CELLS AND 3D-INTEGRATED MICRO-BATTERIES

D. Danilov[1], W.Xu[1], L. Gao[1], V. Pop[2] and P.H.L. Notten[1*]
[1]Eindhoven University of Technology, Eindhoven, the Netherlands
[2]Imec/Holst Centre, Eindhoven, the Netherlands
*Presenting Author: P.H.LNotten @tue.nl

Abstract: Mathematical modeling of three dimensional micro-batteries (3D-MB) and bio-inspired fuel cells (BFC) is important for understanding of the fundamental electrochemical processes, occurring in these devices and is helpful in the design and optimization of personal body area networks (BAN). The combination of the BFC and Lithium (Li)-ion MB improves the energy storage capability and extends the BAN autonomy. In particular it becomes clear that 3D integration is an efficient way to increase the battery surface area thereby reducing the current density and improve electrode and electrolyte kinetics. It leads to significant improvements in battery performance.

Keywords: Bio-inspired fuel cells, 3 dimensional micro-batteries, modeling, thermodynamics and kinetics.

1. INTRODUCTION

Wide application of medical sensors is one of the distinctive features of modern health care. Making medical sensors autonomous increases both the functionality of medical monitoring systems and the comfort level for patients. It is expected that technology will enable people to 'carry' their personal wireless body area network that provides medical functions for the user. This network comprises a series of miniature sensor/actuator wireless nodes each of which has its own energy supply, consisting of energy harvesting and storage systems. Successful realization of such a vision requires innovative solutions to remove the critical technological obstacles for realizing wireless BAN sensor nodes [1]. Clearly, the energy consumption of all the node building blocks, *i.e.* sensor, analog-to-digital converter, microcontroller and radio, needs to be reduced. Subsequently, the autonomy of current battery-powered systems must be extended. A logical way for such extension is combination of BFC as primary energy source with an all-solid-state MB (Fig. 1).

Li-ion MB serves as a buffer to remove apparent power limitations of the BFC devices. The power management circuitry will boost the voltage generated by the BFC, *e.g.* 0.5 V, to the voltage needed to charge the 3D MB, *e.g.* 3-4.2 V voltage range for a conventional Li-ion battery technology. Introduction of rechargeable integrated all-solid-state batteries will enable miniaturization, prevent electrode degradation upon cycling and exclude electrolyte leakage. Planar solid-state thin film batteries are rapidly emerging but reveal several potential drawbacks, such as a relatively

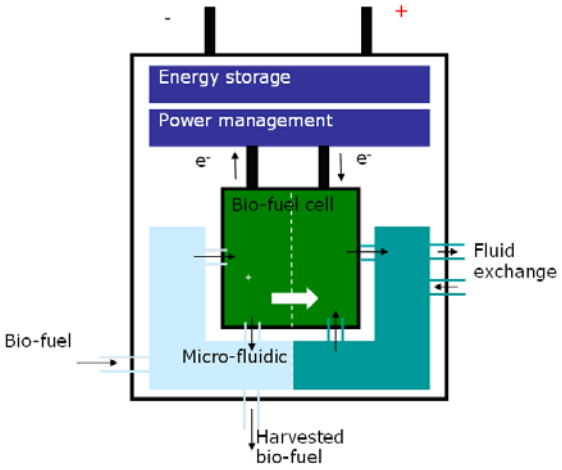

Fig. 1. *Block scheme of an autonomous energy supply unit, consisting of a bio-fuel cell, a power management and a 3D-micro battery.*

low energy density and the use of highly reactive lithium. Thin film Si-intercalation electrodes covered with a solid-state electrolyte are found to combine a high storage capacity of 3500 mAh·g^{-1} with high cycle life, enabling to integrate batteries in Si. Based on the excellent intercalation chemistry of Si, a new 3D integrated all-solid-state battery concept is proposed. High aspect ratio structures, etched in silicon, will yield large surface area batteries with anticipated energy density of about 5 mWh·cm^{-2}·µm^{-1}, *i.e.* more than 3 orders of magnitude higher than that of integrated capacitors.

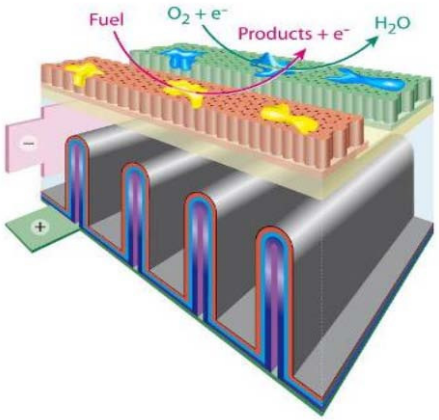

Fig. 2. *The concept of a 3D-integratedMB and an integrated BFC energy harvesting device.*

BAN miniaturization will eventually lead to new integration and packaging technologies, resulting in the integration of 3D-MB energy storage and BFC harvesting devices into single solid-state modules (Fig. 2) [2]. The development and design of suitable Battery Management System (BMS) is another challenging problem. Such system heavily relies on mathematical models [3,4]. Consequently, simulation of the 3D MB and BFC is essential of such research.

2. THEORY

Enzymes are well-known as active and highly specific catalysts. The key-challenge of enzymatic biofuel cell is electron coupling between the enzyme electro-active centres and the electrode [5]. Electrons can transfer between the active sites and the electrode via mediator molecules, denoted as Mediator electron transfer (MET), or via a Direct electron transfer (DET), see Fig. 3a and b correspondingly.

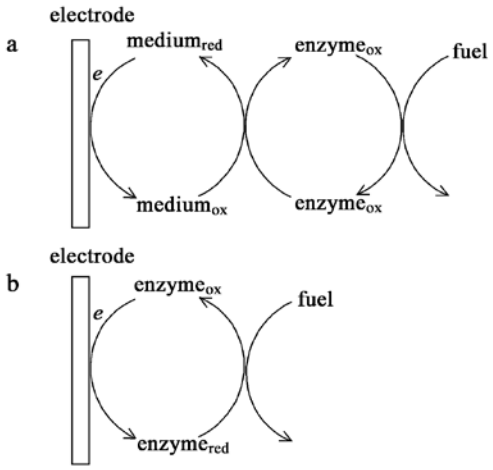

Fig. 3. *Types of electron transfer pathway. (a) Mediated electron transfer (MET). (b) Directed electron transfer (DET).*

A detailed mathematical description of MET-based BFC requires a basic understanding of the (electro)chemical reactions involved. Denote G the glucose, E_{ox} the oxidized enzyme GO(FAD), E_{red} the reduced form of the enzyme GO($FADH_2$), P the gluconolactone, M_{ox}^+ the oxidized mediator (ferrocene cation) Fc^+, and M_{red} the reduced mediator (ferrocene) Fc. The complete reaction sequence given in Fig. 3 can then be written as

$$G + E_{ox} \xrightarrow{k_1} P + E_{red} \tag{1}$$

$$E_{red} + 2M_{ox}^+ \xrightarrow{k_2} E_{ox} + 2M_{red} + 2H^+ \tag{2}$$

$$M_{red} \underset{k_{-3}}{\overset{k_3}{\rightleftarrows}} M_{ox}^+ + e^- \tag{3}$$

The concentration dependencies of all reacting species (c_i) is described by the mass-balance equation

$$\frac{\partial c_i}{\partial t} = -\nabla \cdot \boldsymbol{J}_i, \tag{4}$$

where the Nernst-Planck flux of the reacting species is given by

$$\boldsymbol{J}_i = -D_i \nabla c_i - z_i F D_i c_i E / (RT) \quad e_i \, \mathbf{u} \tag{5}$$

where D_i is the diffusion coefficient of species i [$m^2 \cdot s^{-1}$], R the gas constant (8.314 $J \cdot mol^{-1} \cdot K^{-1}$), F the Faraday constant (96485 $C \cdot mol^{-1}$). T the absolute temperature (K), E the potential gradient [$V \cdot m^{-1}$], z_i the valence number, and $\mathbf{u}$ is the velocity of the electrolyte [$m \cdot s^{-1}$]. The electrolyte velocity can be described by the system of Navier-Stokes equations, according to

$$\begin{cases} \rho \dfrac{\partial \boldsymbol{u}}{\partial t} + \rho(\boldsymbol{u} \cdot \nabla)\boldsymbol{u} = \nabla \cdot \left[-p\boldsymbol{I} + \eta\left(\nabla \boldsymbol{u} + (\nabla \boldsymbol{u})^T\right)\right] \\ \nabla \cdot \boldsymbol{u} = 0 \end{cases} \tag{6}$$

where ρ is the electrolyte density [$kg \cdot m^{-3}$], η the dynamic viscosity [Pa·s] and p is the pressure [Pa]. Numerical solution of Eqs. 4-6, gives the concentration of reacting species c_i in all parts of the BFC, including the electrode surface where the charge transfer reaction (Eq. 3) takes place. The charge transfer kinetics rule of the BFC can be represented by the Butler-Vollmer equation, according to

$$I = I^0 \left[\frac{c^s_{\mathrm{M_{red}}}}{\overline{c}_{\mathrm{M_{red}}}} e^{\alpha \frac{F}{RT}\eta} \quad \frac{c^s_{\mathrm{M^+_{ox}}}}{\overline{c}_{\mathrm{M^+_{ox}}}} e^{-(1-\alpha)\frac{F}{RT}\eta} \right] \tag{7}$$

where $c^s_{\mathrm{M_{red}}}$ and $c^s_{\mathrm{M^+_{ox}}}$ are the surface concentrations of $\mathrm{M^+_{ox}}$ and $\mathrm{M_{red}}$, respectively, $\overline{c}_{\mathrm{M_{red}}}$ and $\overline{c}_{\mathrm{M^+_{ox}}}$ are the corresponding bulk concentrations, α the charge transfer coefficient for reaction 3, η is the overpotential and I^0 is the exchange current density. When large currents are demanded from the BFC, the surface concentrations $c^s_{\mathrm{M_{red}}}$ and $c^s_{\mathrm{M^+_{ox}}}$ may deviate strongly from the corresponding bulk concentrations, thereby increasing the magnitude of the η and, consequently reducing the available power output.

Relaxing the power limitations of BFC can be nicely performed by integration with a rechargeable battery. During recent years a lot of activities in the field of modeling of rechargeable batteries have successfully been performed in the "Energy Materials and Devices" group at Eindhoven University of Technologies (TU/e). These physical- and (electro) chemical-based models include NiCd, NiMH and Li-ion and describe the complex behavior under a wide variety of battery operation conditions in detail (see *e.g.* [3,6-11]). A detailed description of the various processes inside sealed Li-ion batteries by means of our modeling approach generated a much better understanding of the functioning of these complex storage systems.

A schematic representation of a planar solid-state Li-ion battery is shown in Fig. 4 [6,7,12]. The main parts of the Li-ion battery consists of a negative electrode made of lithiated Si, a positive ($LiCoO_2$) electrode and an solid-state electrolyte in between. The main electrochemical storage reactions at the $LiCoO_2$ electrode can be represented by

$$LiCoO_2 \underset{\text{discharge}}{\overset{\text{charge}}{\rightleftarrows}} Li_{1-x}CoO_2 + xLi^+ + xe^-, \quad (0 \le x \le 0.5) \tag{8}$$

describing the extraction of Li^+ ions from the positive electrode during charging and the insertion of these ions during discharging. The corresponding reactions at the negative, Si-based, electrode can be described by

$$Si + yLi^+ + ye^- \underset{\text{discharge}}{\overset{\text{charge}}{\rightleftarrows}} Li_ySi, \tag{9}$$

with maximal identified composition $Si_{15}Li_4$.

Electrochemical kinetics rules applied to the main storage reactions Eqs. (8-9) lead to well-known expressions for the overpotential of the charge transfer

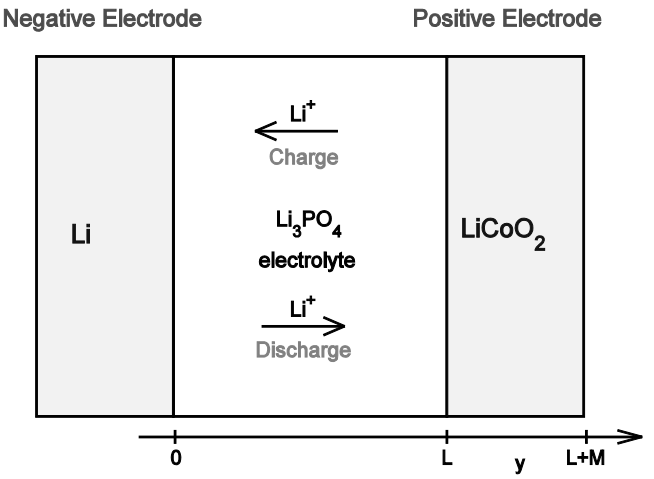

Fig.4. *Schematic representation of a planar all-solid-state Li-ion battery.*

reaction. *E.g.* the kinetic overpotential $\eta^{ct}_{LiCoO_2}$ for the positive electrode is given by

$$I_{LiCoO_2} = I^0_{LiCoO_2} \left[\frac{c^s_{LiCoO_2}}{\overline{c}_{LiCoO_2}} e^{\alpha_{LiCoO_2}\frac{F}{RT}\eta^{ct}_{LiCoO_2}} \frac{c^s_{CoO_2} c^s_{Li^+}}{\overline{c}_{CoO_2}\overline{c}_{Li^+}} e^{-(1-\alpha_{LiCoO_2})\frac{F}{RT}\eta^{ct}_{LiCoO_2}} \right] \tag{10}$$

where I_{LiCoO_2} is the current transferred at the surface of the positive electrode and α_{LiCoO_2} is the charge transfer coefficient for reaction 8.

Another sizable contribution into the total overpotential comes from the electrolyte. The ionically conductive solid-state electrolytes play an important role in the solid-state battery design (see [13,14]) and are known to be responsible for the sizable part of the total battery overpotential. The movement of charge carriers through the electrolyte layers can be described by the mass-balance equation

$$\frac{\partial c_i}{\partial t} = -\nabla \cdot \boldsymbol{J}_i + r \tag{11}$$

with the non-zero term r, representing the charge carriers generation/recombination reaction. When the concentration of all charge carriers, including Li^+ ions is obtained, the mass-transfer overpotential across the electrolyte can be calculated, according to

$$\eta^{mt}_{Li^+}(t) = \frac{RT}{F} \ln\left(\frac{c_{Li^+}(L,t)}{c_{Li^+}(0,t)}\right) \int_0^L E(y,t)\,dy, \tag{12}$$

where $E(y,t)$ is the electric field across the electrolyte.

Finally, solving the diffusion problem for Li in the electrode, the diffusion overpotential can be calculated.

3. RESULTS AND DISCUSSIONS

Modelling the current-voltage curves of the anode of the BFC is illustrated in Fig. 5. Two clearly visible areas can be discerned: a steep kinetically controlled part and a flat diffusion-controlled part. In the diffusion controlled area even very small changes in the magnitude of the current lead to a sharp increase of the overpotential and, therefore, to a significant reduction in power output. Experimental confirmations of this fact are well known (see [15]). Removing the power limitations of the BFC can be performed by integration with the secondary energy storage device, preferably an all-solid-state Li-ion battery.

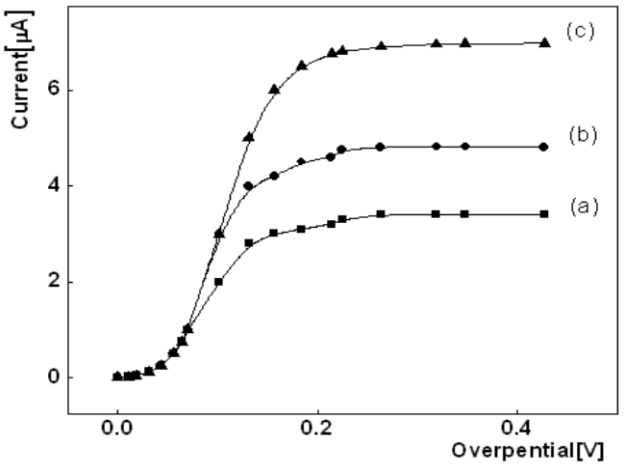

Fig. 5. *Simulation of current-voltage curves of the anode of a BFC in a buffered electrolyte (PBS pH 7.2) containing 1 mM Ferrocene as mediator. (a) Ferrocene+Gox +1 mM Glucose; (b) Ferrocene+Gox +10 mM Glucose; (c) Ferrocene+Gox +20 mM Glucose.*

A mathematical model of a planar solid-state Li-ion battery [12] reveals a good agreement with the experimental data. Fig. 6 shows the agreement between the simulated (red lines) and experimentally observed (blue dots) charge and discharge voltages for a planar solid-state Li-ion battery. The applied discharge rates are 3.2, 6.4, 12.8, 25.6 and1 51.2 C. It is remarkable to see that these thin film batteries can be discharged with extremely high currents up to 51.2 C-rate. These results prove the high power capability of all-solid-state batteries which makes them interesting candidates for integration in BAN.

Mathematical modeling provides deep insight into the functioning of all-solid state Li-ion batteries. In particular the development of concentration profiles of the Li^+ ions in all parts of the battery becomes known. Fig. 7a illustrates the development of the Li^+ concentration profiles inside the solid-state (Li_3PO_4- type) electrolyte, while Fig. 7b shows development of such profile in the positive

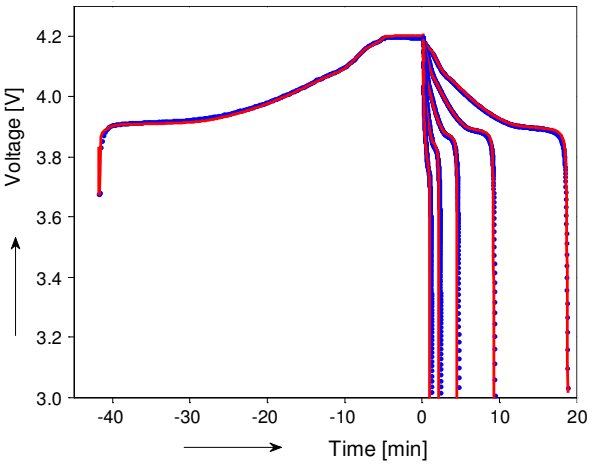

Fig. 6. *Voltage profiles of an solid-state Li-ion battery during charge and discharges with various C-rates.*

electrode during discharge with high 51.2 C-rate. It is clearly visible that sizable concentration gradients are build up in both parts of the battery. Those concentration gradients are responsible for high overpotentials and, therefore for the reduction in power output. Therefore an increase in power delivery is essential.

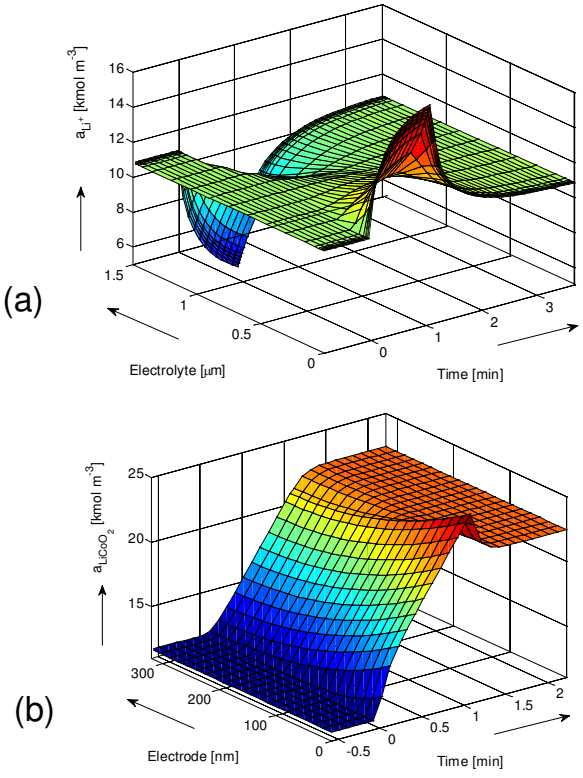

Fig.7. *Development of concentration profiles during (a) 51.2 C discharge in the solid-state electrolyte and (b) in the $LiCoO_2$ electrode.*

Thin-film all-solid-state Li-ion batteries are currently under development by several start-up companies. However, to increase the energy density of these micro-batteries further and to ensure a high power delivery, 3D-designs are essential.

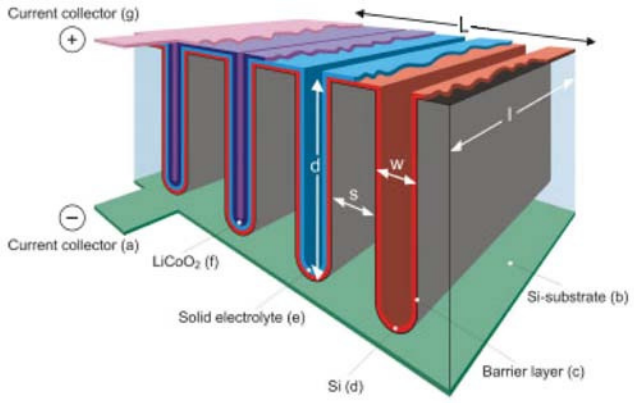

Fig. 8. *Geometric definitions of 3D trenches.*

Notten *et al.* [16] therefore proposed to use this material as substrate material for the integration of all-solid-state micro-batteries (Fig. 8). The first step in this approach is to use an anisotropic etching method to manufacture a three-dimensional structure in the substrate to enlarge the surface area. As etching techniques, either electrochemical [17] or reactive ion etching [18] can be applied. The etched 3D-structure typically consists of trenches [16], but various other geometries can also be made, like pores or pillars [19]. Commonly used dimensions for etched trench structures vary from 1 µm to 30 µm in width and 10-100 µm in depth. The surface area enhancement (Fig. 9) can be calculated for a trench structure using

$$g_A = 1 + 2d\frac{L-s}{L(w+s)} \qquad (13)$$

in which d is the trench depth, w the width, s the spacing between the trenches and L the total footprint length of the battery structure, see Fig. 8 [2].

A surface area enhancement of, for example, 28 can be calculated using d = 135 µm, w = 5µm and s = 5µm for single-sided integration [20] and this value doubles for double-sided integration. Based on standard etching technology these dimensions were already shown to be feasible.

Mathematical modeling can help in finding out how the 3D-structuring improves the performance of the energy storage devices. Suppose that battery surface area is increased while the amount of electrode material is kept constant. Consequently,

1. The current density will decrease, which will positively affect both the mass-transfer in the electrolyte and the surface kinetics and
2. The effective diffusion inside the electrode will increase according to $\kappa = D/l^2$.

In combination, these effects result in a significant decrease in the total battery overpotential.

Fig. 10a shows the decrease in the battery overpotential when geometrical area gain is, for example, 2, *i.e.* $g_A = 2$, and the (dis)charge currents

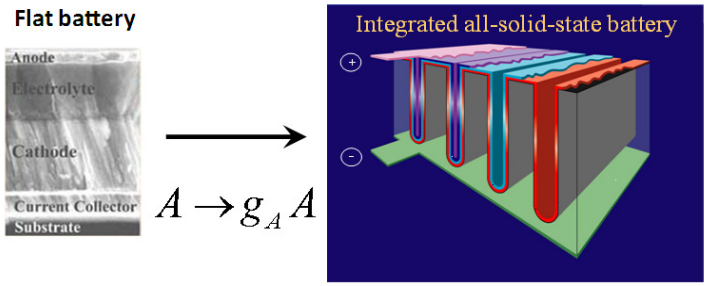

Fig. 9. *The concept of geometrical area gain.*

are constant. Blue dots represent measured voltage for the flat battery, where $g_A = 1$. The green line shows equilibrium battery voltage, i.e. "ideal" case when no overvoltages are present. Two red lines show simulated battery voltages for planar case ($g_A = 1$) and 3D integrated case ($g_A = 2$). The red arrows show the direction of the overpotential change, which is significantly reduced. Fig. 10b shows the influence of a further surface area enlargement on the battery

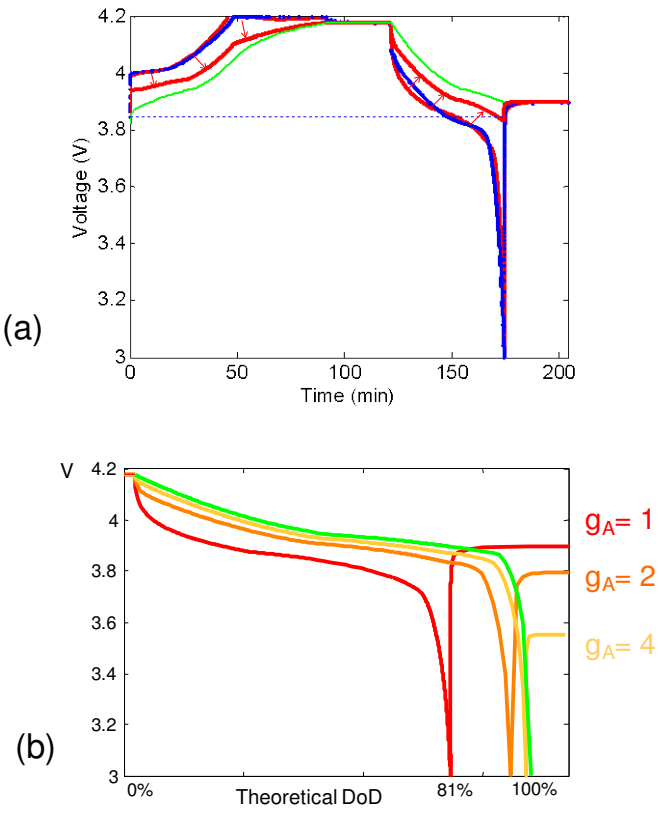

Fig. 10. *Reduction of the overpotentials of the flat Li-ion battery resulting from 3D-structuring (a) and improvements in the kinetics as function of the surface area enlargement (b).*

performance. For the flat thin-film battery only about 80% of available capacity can be utilized due to voltage decrease (red curve). However increasing the surface area 4 times (yellow curve) reduces the power limitation practically to zero under these conditions,

almost extracting the theoretical amount of charge (green curve).

3D integration can be applied in different ways. Instead of increasing the surface area and keeping the amount of electrode material constant the alternative would be to reduce the layer thickness. The resulting battery would obviously reveal an increased storage capacity proportional to the geometrical area gain (g_C). Fig. 11 illustrates both approaches. The red straight line show the linear increase in storage capacity in such battery as function of area enlargement. The blue line illustrates the decrease of the overpotential. From the definition of power it is apparent that power loss of the battery is directly proportional to the magnitude of the overpotential, thus an increase in surface area enlargement is a direct way to reduce battery power limitations.

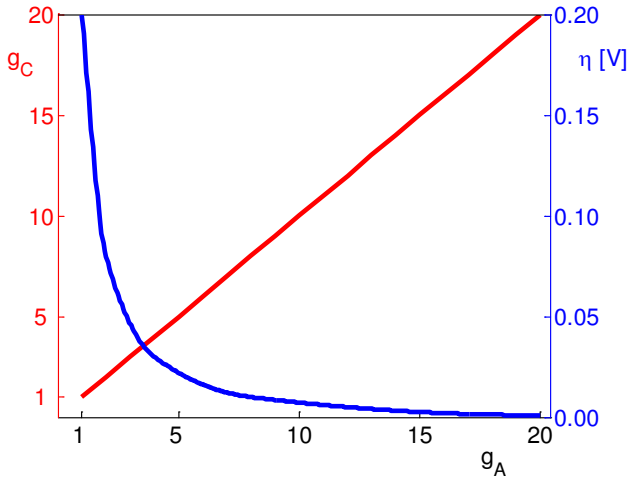

Fig. 11. *Relation between relative capacity increase (red line/scale) and overpotential (blue line/scale) as function of geometrical area gain (current is kept constant in the simulations).*

4. CONCLUSIONS

- Combination of the BFC and 3D Li-ion MB extends the BAN device autonomy.
- 3D integration is an effective way to increase the battery surface area.
- 3D integration reduces the current density and thus improves electrolyte kinetic.
- 3D integration may improve electrode kinetics thus reduce diffusion limitations.
- 3D integration also may be used to increase battery capacity.
- Significant improvement in battery performance is expected due to large improvement in electrode kinetic.
- Mathematical modeling provides efficient tools for deep understanding of fundamental electrochemical processes occurring in BCF-s and MB-s.

ACKNOWLEDGEMENTS

The authors would like to thank the European Union (FP7) within the framework of the Superlion project for their financial support.

REFERENCES

[1] V. Pop *et. al.*, Power optimization for Wireless Autonomous Transducer Solutions, in *The 8th International Workshop on Micro and Nanotechnology for Power Generation,* 8, 141, (2008).
[2] J. Oudenhoven, L. Baggetto and Peter H.L. Notten, Adv. Ener. Mat., (2010).
[3] H.J. Bergveld, W.S. Kruijt and P.H.L. Notten, *Battery Management Systems – Design by Modelling, Philips Research Book Series, Kluwer Academic Publishers, Boston, vol. 1,* (2002).
[4] H.J. Bergveld, D. Danilov, V. Pop, P.P.L. Regtien, P.H.L. Notten, State-of-Charge Determination Mainly for Li Batteries, in *Encyclopedia of Electrochemical Power Sources,* (2009).
[5] J. A. Cracknell, K.A. Vincent, F.A. Armstrong, Chem. Rev., 108, 2439-2461, (2008).
[6] V. Pop, H.J. Bergveld, D. Danilov, P.P.L. Regtien, P.H.L. Notten, *Battery Management Systems: Accurate State-of-Charge Indication for Battery-Powered Applications, Springer,* (2008).
[7] D. Danilov and P.H.L. Notten, Electrochim. Acta, 53 (17), 5569, (2008).
[8] D. Danilov and P.H.L. Notten, J. Power Sources, 189, 303, (2009).
[9] W.S. Kruijt, P.H.L. Notten and H.J. Bergveld, J. Electrochem. Soc., 145, 3764, (1998).
[10] P.H.L. Notten, W.S. Kruijt and H.J. Bergveld, J. Electrochem. Soc., 145, 3774, (1998).
[11] H.J. Bergveld, W.S. Kruijt and P.H.L. Notten, J. Power Sources, 77, 143, (1999).
[12] D. Danilov and P.H.L. Notten, "Modeling all-solid-state Li-ion batteries", J. Electrochem. Soc., in press.
[13] J.B. Bates, N.J. Dudney, G.R. Gruzalski, R.A. Zuhr, A. Choudhury, C.F. Luck and J.D. Robertson, J. Power Sources, 43–44, 103, (1993).
[14] J.B. Bates, N.J. Dudney, D.C. Lubben, G.R. Gruzalski, B.S. Kwak, Yu Xiaohua and R.A. Zuhr, J. Power Sources, 54, 58, (1995).
[15] W.Xu, L. Gao, D. Danilov, V. Pop, P.H.L. Notten, *Bio-inspired fuel cells for miniaturized Body-Area-Networks Applications*, Proceedings of The 10th International Workshop on Micro and Nanotechnology for Power Generation and Energy Conversion Applications, Dec. 1, Leuven, Belgium, (2010).
[16] P. H. L. Notten, F. Roozeboom, R. A. H. Niessen, L. Baggetto, Adv. Mater., 19, 4564, (2007).
[17] J. van den Meerakker, R. J. G. Elfrink, F. Roozeboom, J. Verhoeven, *J. Electrochem. Soc.*, *147*, 2757, (2000).
[18] F. Laermer, A. Urban, *Microelectr. Eng.*, *67-68*, 349, (2003).
[19] L. Baggetto, J. F. M. Oudenhoven, T. van Dongen, J. H. Klootwijk, M. Mulder, R. A. H. Niessen, M. de Croon, P. H. L. Notten, J. Power Sources, 189, 402, (2009).
[20] L. Baggetto, R. A. H. Niessen, F. Roozeboom, P. H. L. Notten, Adv. Funct. Mater., 18, 1057, (2008).